

Supporting Information

Colloidal Spherical Quantum Wells with Near-Unity Photoluminescence Quantum Yield and Suppressed Blinking

*Byeong Guk Jeong,[†] Young-Shin Park,^{‡,¶} Jun Hyuk Chang,[^] Ikjun Cho,^Δ Jai Kyeong Kim,[§]
Heesuk Kim,[§] Kookheon Char,[^] Jinhan Cho,^Δ Victor I. Klimov,[‡] Philip Park,^{#,*} Doh C. Lee^{‡,*}
and Wan Ki Bae^{§,*}*

[†]Department of Chemical and Biomolecular Engineering, KAIST Institute for the Nanocentury, Korea Advanced Institute of Science and Technology (KAIST), 291 Daehak-ro, Yuseong-gu, Daejeon 34141, Republic of Korea, [‡]Chemistry Division, Los Alamos National Laboratory, Los Alamos, New Mexico 87545, United States, [¶]Center for High Technology Materials, University of New Mexico, Albuquerque, New Mexico 87131, United States, [^]School of Chemical and Biological Engineering, The National Creative Research Initiative Center for Intelligent Hybrids, Seoul National University, 1 Gwanak-ro, Gwanak-gu, Seoul 08826, Republic of Korea, ^Δ Department of Chemical and Biological Engineering, Korea University, 145 Anam-ro,

Seongbuk-gu, Seoul 02841, Republic of Korea, §Photoelectronic Hybrids Research Center,
Korea Institute of Science and Technology (KIST), 14-gil 5 Hwarang-ro, Seongbuk-gu, Seoul
02792, Republic of Korea, #Department of Chemistry and Biochemistry, University of
California, Los Angeles, California 90095, United States

KEYWORDS. spherical quantum well, near-unity photoluminescence quantum yield, coherently
strained heterostructure, misfit defect, critical thickness

1. Photoluminescence quantum yields of nanocrystals

Photoluminescence quantum yields (PL QYs) of synthesized CdSe/CdS core/shell (C/S) NCs and CdS/CdSe/CdS core/spherical quantum well/shell (SQW) NCs are characterized at the excitation wavelength (450 nm) with the absolute PL QY measurement system (QE-2100, Otsuka Photonics) that utilizes an integrating hemisphere, a low stray light spectrometer and fluorescent re-excitation elimination. To correlate the heterostructure parameters with the final optical properties, we plot PL QYs of C/S NCs ($r = 1.5$ nm) and SQW NCs ($r/l = 1.3/0.9$ nm) as a function of the CdS shell thickness (Figure S1). PL QYs of CdSe($r = 1.5$ nm)/CdS C/S NCs are also taken from literatures for statistics.¹⁻¹⁵

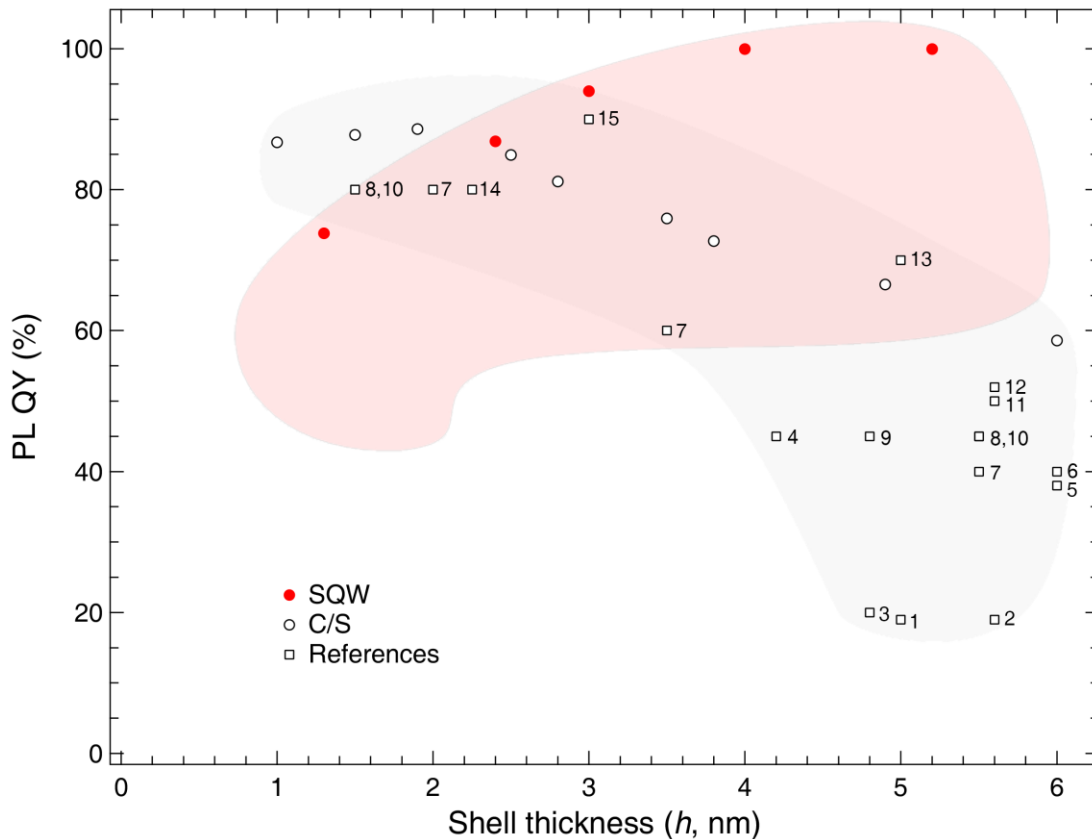


Figure S1. PL QYs of CdSe/CdS (C/S) and CdS/CdSe/CdS (SQW) NCs as a function of the CdS shell thickness.

2. Synthesis and characterization of nanocrystals

Chemicals: Cadmium oxide (CdO, 99.95 %, metals basis), zinc acetate (Zn(acet)₂, 99.999%, metals basis) and tri-n-octylphosphine (TOP, technical grade, 90%) were purchased from Alfa Aesar. Se (99.99 %, powder), S (99.998 %, powder), oleic acid (OA, 90 %), 1-dodecanethiol (DDT, ≥ 98 %), 1-octadecene (ODE, 90 %, technical grade) and myristic acid (MA, ≥ 99 %) were purchased from Sigma Aldrich. All organic solvents were acquired from Daejung (Korea). All chemicals were used as received.

Precursors: All NC syntheses were carried out using the Schlenk line technique under Ar atmosphere. Cationic precursors [0.5 M cadmium oleate (Cd(OA)₂) and 0.5 M zinc oleate (Zn(OA)₂] were prepared by dissolving CdO (100 mmol) (or Zn(acet)₂) in mixed solvent of OA (100 mL) and ODE (100 mL) under Ar atmosphere at 250 °C for 1 hr, degassing at 110 °C for 2 hr, and filling with Ar. Anionic precursors [2 M TOPSe and 2 M TOPS] were prepared by dissolving selenium and sulfur power (20 mmol) in 10 mL of TOP under Ar atmosphere at 100 °C for 1 hr.

Synthesis of CdS/CdSe/CdS SQW NCs: For preparing CdS ($r = 1.3$ nm) seeds, Cd(OA)₂ (0.3 mmol) was added in 3-neck flask containing of ODE (9 mL) and heated up to 270 °C. At the elevated temperature, the 0.25 M S-ODE (0.5 mL, S dissolved in ODE) precursor was rapidly injected into the reaction vessel to create nuclei and cooled down to 250 °C for further growth. The reaction was proceeded for 10 min. Larger sized CdS ($r = 1.5$ or 2.0 nm) seeds were synthesized by adding mixed Cd and S precursors (0.1 M Cd(OA)₂ and 0.1 M TOPS) into the reaction flask containing CdS ($r = 1.3$ nm) seeds at a rate of 5 mL/hr at 250 °C. After the precursor injection, the reaction flask was maintained at the elevated temperature for more 10 min and cooled down to room temperature to complete the reaction. The resultant NCs were

purified twice by precipitation (ethanol)/redispersion(toluene) method. For CdSe emissive layer growth, the desired amount of mixed Cd and Se precursors [0.1 M Cd(OA)₂ and 0.1 M TOPSe] diluted in ODE was injected into the 3-neck flask containing CdS seeds (0.1 g) and ODE (10 mL) at 300 °C at a rate of 5 mL/hr. After injecting the precursors, the reaction flask was cooled down to room temperature and the CdS/CdS NCs were purified twice. For CdS shelling, CdS/CdSe NCs (0.1 g) and ODE (10 mL) were loaded into the flask and 0.5 M Cd(OA)₂ and 0.5 M DDT were added separately into the reaction solution at a rate of 2 mL/hr. The reaction temperature was maintained at 300 °C for the entire CdS shelling process and cooled down to room temperature to stop the reaction. Final products were purified twice and dispersed in toluene for further characterization.

Synthesis of CdSe/CdS core/shell NCs: CdSe NCs ($r = 1.5$ nm) were synthesized by the previously reported method.¹⁰ For CdS shelling, CdSe NCs (0.1 g) were added to a 3-neck flask containing ODE (8 mL) and 0.5 M Cd(OA)₂ (0.6 mL) at 300 °C under Ar atmosphere. At the elevated temperature, 0.5 M Cd(OA)₂ and 0.5 M 1-DDT precursors were injected separately into the reaction vessel at a rate of 2 mL/hr. The reaction temperature was maintained at 300 °C throughout the CdS shelling process. The resultant NCs were purified twice by the precipitation/redispersion method and dispersed in toluene for further characterization.

Synthesis of CdSe/Cd_xZn_{1-x}S core/shell NCs: Detailed synthesis and structural characterization was reported previously.¹⁶ CdO (1 mmol), MA (3 mmol) and ODE (15 mL) were loaded in 3 neck flask and heated up to 300 °C under the inert conditions to form Cd(MA)₂ complex. After reactants turned to be optically clear, 2 M TOPSe (0.25 mL) was rapidly injected into the reaction flask to form CdSe cores. After 3 min of reaction, 3 mL of the 0.5 M Zn(OA)₂ precursor and DDT (1 mmol) were added separately within 1 min. The reaction was preceded for 30 min to

form $\text{Cd}_{0.6}\text{Zn}_{0.4}\text{S}$ inner shell. 0.5 M $\text{Cd}(\text{OA})_2$ (2 mL), 0.5 M $\text{Zn}(\text{OA})_2$ (4 mL) and 2 M TOPS (1.5 mL) were added into the reaction flask within 1 min for $\text{Cd}_{0.5}\text{Zn}_{0.5}\text{S}$ shelling and the reaction proceeded for 10 min. Final products were repeatedly purified and dispersed in toluene.

Optical Characterization: The absorption and PL spectra of NC dispersions were measured with the V-670 UV-Visible/NIR spectrometer (Jasco) and the Fluoromax-4 spectrometer (Horiba). The absolute PL QYs of solution and film samples were measured at the excitation wavelength (450 nm) with the QE-2100 (Otsuka Photo Electronics). For measuring PL decay dynamics, the samples were excited at 450 nm (pulse width = 80 ps) at a repetition rate of 2.5 MHz, and PL dynamics were resolved using a time-correlated single-photon counting (TCSPC) system that consists of avalanche photodiodes (temporal resolution = 350 ps) and a single channel analyzer (with a Picoquant Timeharp 260) with a 50 ps binning time.

Structural Characterization: The sizes of NCs were characterized with transmission electron microscopy (Tecnai TF30 ST). The morphology of NC films was analyzed with scanning electron microscopy (Hitachi S-4300).

Film Stability Test: NC films were stored in an oven at 200 °C. For characterization, the films were cooled down naturally to room temperature. After characterization, films were again moved to the oven.

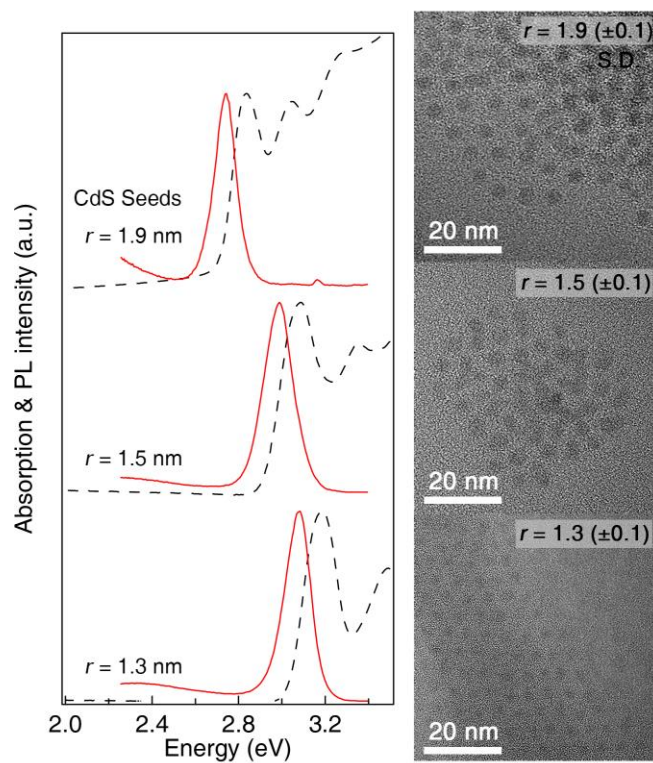


Figure S2. Absorption and PL spectra and (left) TEM images (right) of CdS seeds with different radii.

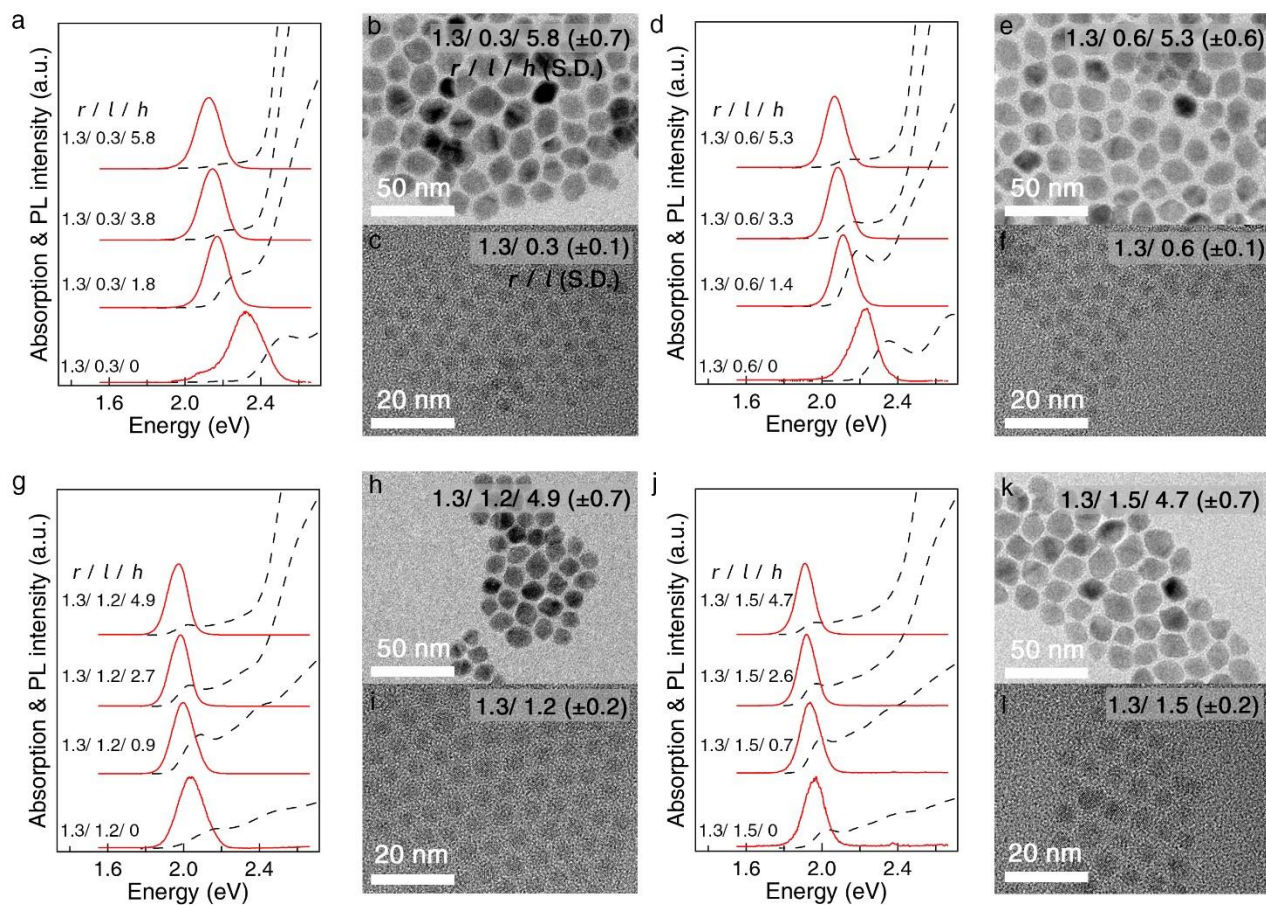


Figure S3. (a, d, g, and j) Absorption and PL spectra and (b, c, e, f, h, I, k and l) TEM images of CdS/CdSe/CdS SQW NCs with fixed CdS seed radius ($r = 1.3$ nm) but different emissive layer ($l = 0.3, 0.6, 1.2$ and 1.5 nm) and shell thicknesses.

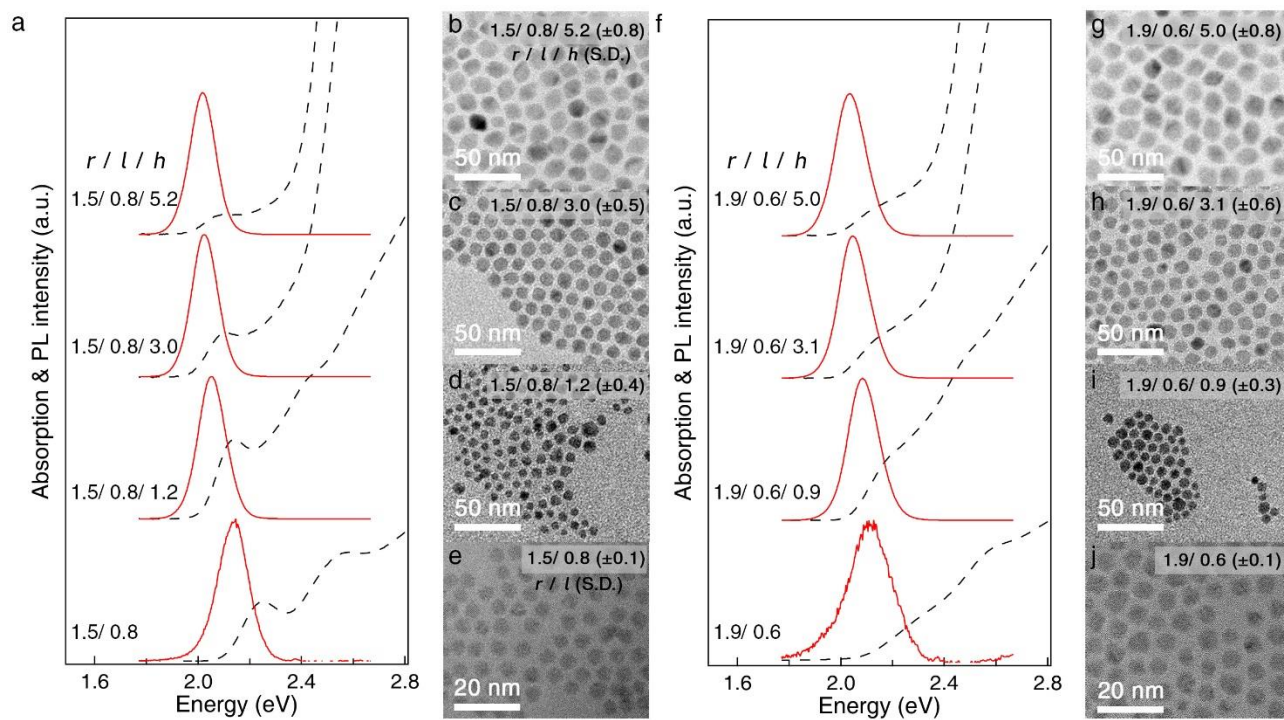


Figure S4. (a and f) Absorption and PL spectra and (b-e and g-j) TEM images of CdS/CdSe/CdS SQW NCs with different CdS core radii ($r = 1.5$ or 1.9 nm) and similar volumes of the CdSe emissive layer. The NC dimensions (r , l , and h) are indicated in the figure.

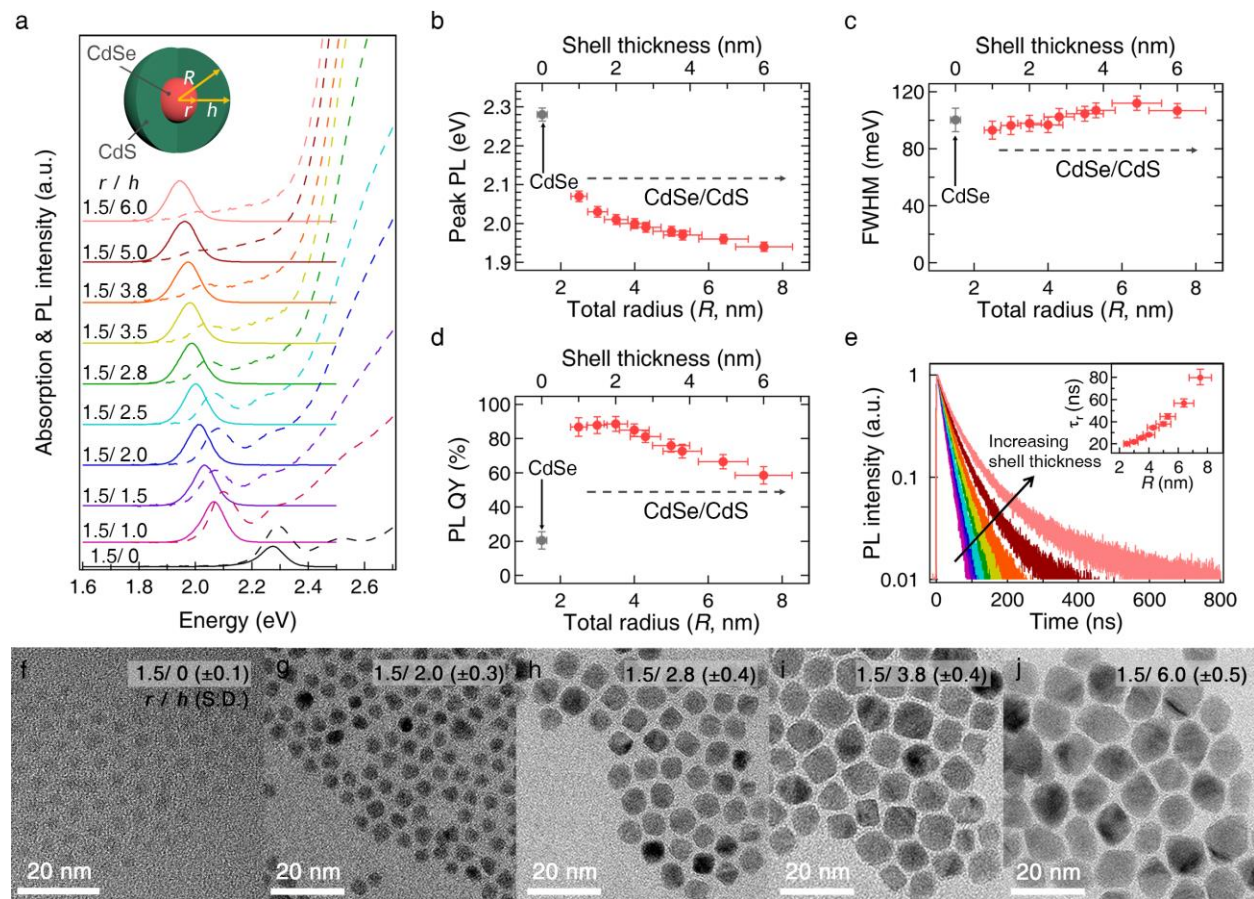


Figure S5. Structural and optical characteristics of CdSe/CdS core/shell NCs with varying shell thicknesses. (a) Absorption, PL spectra and schematic illustration of CdSe/CdS core/shell (C/S) NCs; r , h , and R denote the radius of CdSe core, the thickness of CdS shell and the total radius, respectively. (b) Peak PL energies in eV, (c) FWHM, (d) PL QYs, (e) PL decay dynamics (inset: single-exciton radiative recombination time (τ_r)), and (f-j) TEM images of CdSe/CdS C/S NCs with varying CdS shell thicknesses ($r = 1.5$ nm, $h = 0, 2.0, 2.8, 3.8$ and 6.0 nm).

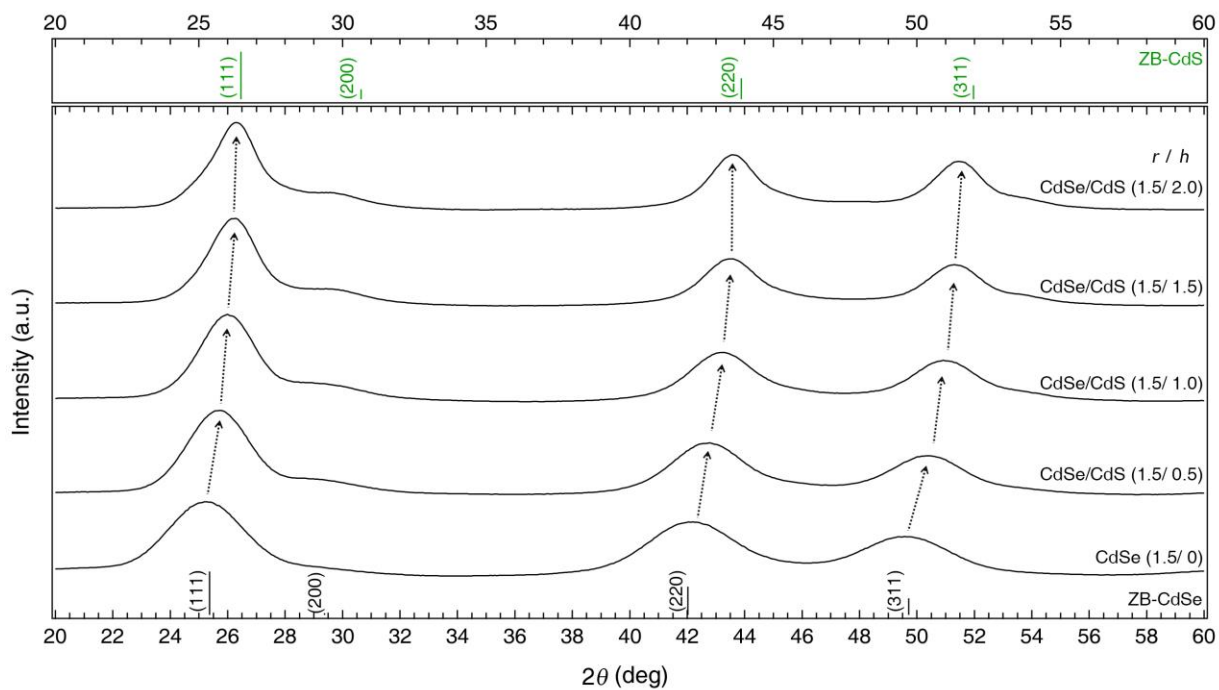


Figure S6. X-ray diffraction (XRD) patterns of CdSe NCs ($r = 1.5$ nm) and CdSe/CdS core/shell NCs with varying shell thickness ($r = 1.5$ nm, $h = 0.5, 1.0, 1.5, 2.0$ nm). XRD patterns of bulk zincblende (ZB) CdSe (bottom) and CdS (top) are shown for comparison. XRD patterns are vertically shifted for visual clarity.

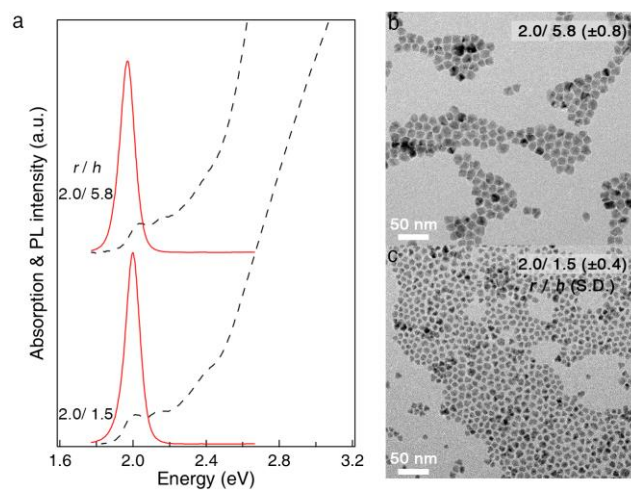


Figure S7. (a) Absorption and PL spectra and (b,c) TEM images of CdSe ($r = 2.0$ nm)/Cd_xZn_{1-x}S ($h = 1.5$ and 5.8 nm) NCs.

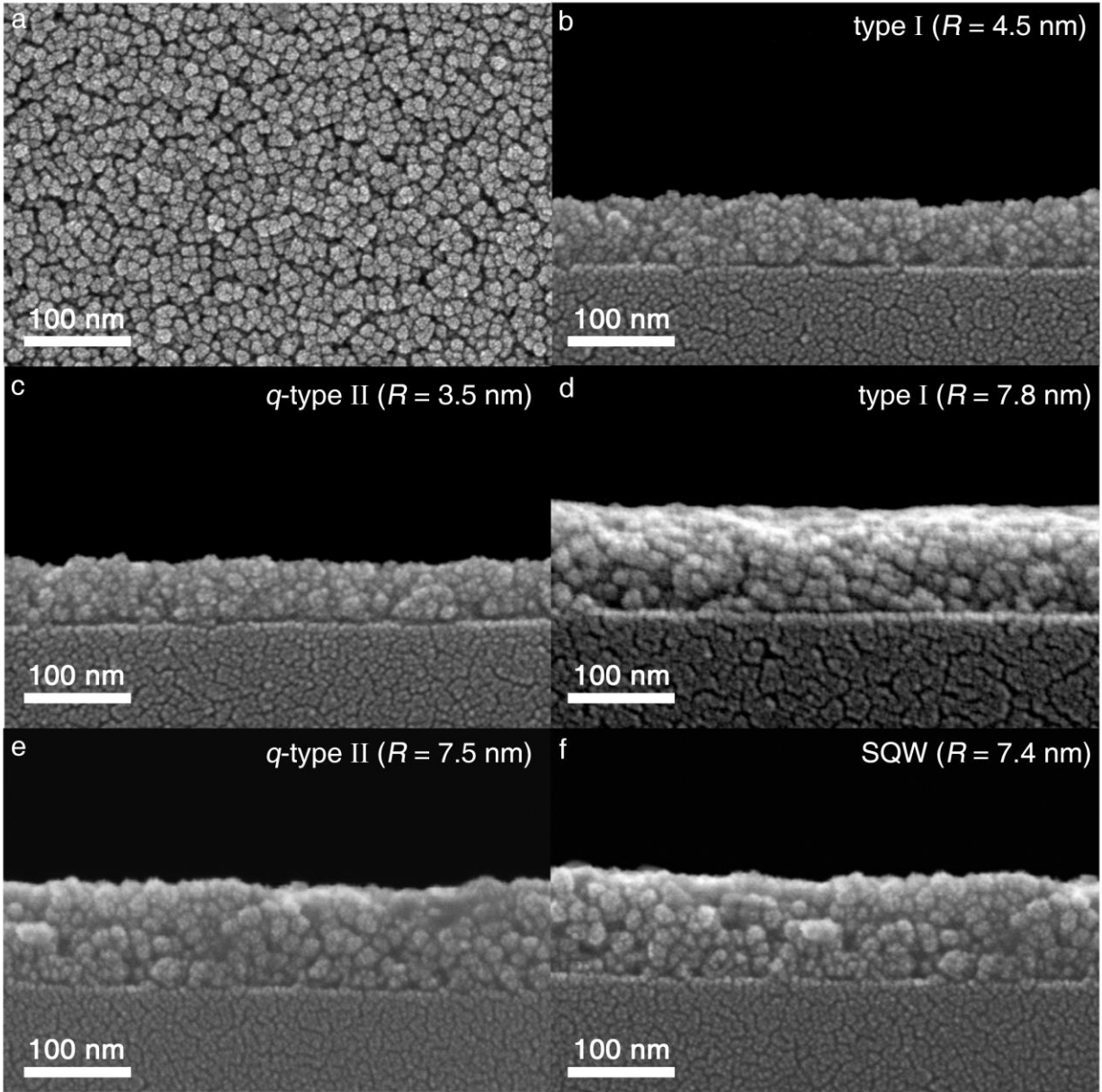


Figure S8. (a) FE-SEM images of a SQW NC film and (b-f) cross-sectional FE-SEM images of films made of various types of NCs with the indicated total radius R . CdS ($r = 1.3$ nm)/CdSe ($l = 0.9$ nm)/CdS ($h = 5.2$ nm), CdSe ($r = 1.5$ nm)/CdS ($h = 2.0$ and 6.0 nm) and CdSe ($r = 2.0$ nm)/Cd_xZn_{1-x}S ($h = 2.5$ and 5.8 nm) NCs are denoted as ‘SQW’, ‘type I’ and ‘ q -type II’.

3. Calculation of critical thickness of shell layer for nanocrystals

To obtain the critical thickness of the CdS shell layer on the CdSe core NCs, we utilized Matthew and Blakeslee's equilibrium theory.¹⁷ The critical thickness of thin film on substrate can be calculated as:

$$h_c = \frac{b}{2\pi f} \frac{(1-\nu \cos^2 \alpha)}{(1+\nu) \cos \lambda} \left(\ln \frac{h_c}{b} + 1 \right) \quad (1)$$

where b is the magnitude of Burgers vector ($b = 1/2\langle 110 \rangle$ for FCC crystals), f is the lattice mismatch between the film and the substrate ($\sim 4.2\%$), ν is the Poisson ratio (0.454 for zb-CdSe (111) plane)¹⁸ and α is the angle between the dislocation line and its Burgers vector (0.667).¹⁹ λ is the angle between the slip direction and the direction in the film plane which is perpendicular to the line of intersection of the slip plane and the interface (45°).¹⁷ As a result, the calculated critical thickness of the CdS layer on the CdSe core is 3.3 nm. Although 3-dimensional nanocrystals have curvatures unlike the thin film, the theoretical value is similar to that obtained from the experiment (*ca.* 2.5 nm). On the other hand, due to the smaller lattice mismatch ($\sim 4.0\%$), the calculated critical thickness of the CdSe layer grown on top of the CdS core is 3.6 nm.

4. Calculation of electron-hole overlap integral (Θ_{e-h}) for nanocrystals

In Fig. 5b, the PL QYs of SQW NCs having 1.3/0.3/5.8 nm and 1.3/1.5/4.7 nm dimensions (CdS core radius/CdSe layer thickness/CdS shell thickness) are 65.5% and 91%, respectively. We speculate that the drop in the PL QY for SQW NCs with a thinner CdSe emissive layer (1.3/0.3/5.8 nm) compared to other SQW NCs is due to the reduced radiative recombination rate resulting from the reduced electron-hole overlap integral. To support this assessment, we perform theoretical modeling.

The calculations are based on a finite-difference method (FDM), implemented with a custom code, written using a Python program. Ground state electron and hole wave functions and their eigen energies are found by solving the Schrodinger's equation in the two band K•P formalism.²⁰⁻²¹ NCs are modeled using cylindrical coordinates with inclusion of rotational symmetry. Using this method, full 3D calculations can be realized while the memory requirements are greatly reduced compared to the approach utilizing a 3D mesh.²² The K•P formalism is following.

$$\left(H_0 + \frac{\hbar}{m_0} K \cdot p \right) u_{n,k}(r) = \left(E_n(k) - \frac{\hbar^2 k^2}{2m_0} \right) u_{n,k}(r)$$

where $u_{n,k}$ is the cell periodic part of the Bloch function ($\phi_{n,k}(r) = e^{ik \cdot r} u_{n,k}(r)$). This form can be changed to

$$\sum_{n'} \left\{ \left(E_n(0) + \frac{\hbar^2 k^2}{2m_0} \right) \delta_{n,n'} + \frac{\hbar}{m_0} K \cdot p_{n,n'} \right\} a_{n'} = E_n(k) a_n$$

where a_n is the coefficient of the basis function $\psi = \sum_n a_n \phi_{n,k}(r)$.

By merging the all other bands' contribution into the simple parameter (α_e or α_h), this matrix will be simply solved by the following expression.

$$\begin{vmatrix} \frac{\alpha_e \hbar^2}{2m_o} \nabla^2 + \frac{E_g}{2} + U_e(x) - E & \frac{\hbar}{m} \hat{k} \cdot P_{nm} \\ \frac{\hbar}{m} \hat{k} \cdot P_{nm} & \frac{\alpha_h \hbar^2}{2m_o} \nabla^2 - \frac{E_g}{2} - U_h(x) - E \end{vmatrix}$$

The wavefunctions of electrons (blue) and holes (red) are shown in Fig. S9. The overlap integral ($\langle \phi_e | \phi_h \rangle^2$) of the thin-CdSe-layer SQW NC (1.3/0.3/5.8 nm) is 0.17, which is lower than that of the thick-CdSe-layer SQW NC (1.3/1.5/4.7 nm) wherein $\langle \phi_e | \phi_h \rangle^2 = 0.37$. Consequently, the radiative recombination rate of the thin-CdSe-layer SQW NC is 55% lower than that of the thick-layer SQW NC.

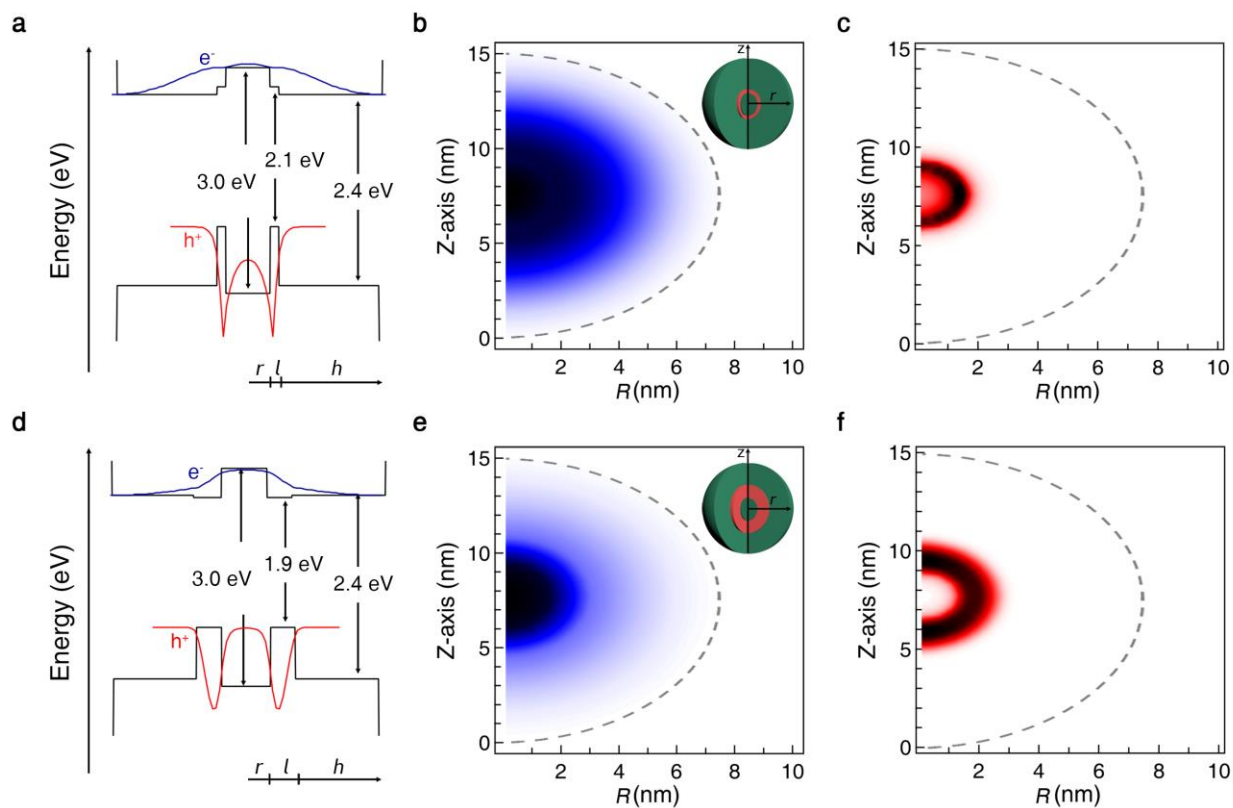


Figure S9. Electron and hole wavefunctions of (a-c) the thin-CdSe-layer SQW NC (1.3/0.3/5.8 nm) and (d-f) the thick-CdSe-layer SQW NC (1.3/1.5/4.7 nm). Cross-section of wavefunctions at $r = 0$ are shown in (a) and (d) where solid-blue and solid-red lines represent electron and hole wavefunctions, respectively. Probability distribution functions of (b,e) electron and (c,f) hole in each SQW NCs are presented. Gray-dash lines indicate the NC boundary.

References

1. Spinicelli, P.; Buil, S.; Quélin, X.; Mahler, B.; Dubertret, B.; Hermier, J. P., Bright and Grey States in CdSe-CdS Nanocrystals Exhibiting Strongly Reduced Blinking. *Phys. Rev. Lett.* **2009**, *102*, 136801.
2. Htoon, H.; Malko, A. V.; Bussian, D.; Vela, J.; Chen, Y.; Hollingsworth, J. A.; Klimov, V. I., Highly Emissive Multiexcitons in Steady-State Photoluminescence of Individual “Giant” CdSe/CdS Core/Shell Nanocrystals. *Nano Lett.* **2010**, *10*, 2401-2407.
3. Pal, B. N.; Ghosh, Y.; Brovelli, S.; Laocharoensuk, R.; Klimov, V. I.; Hollingsworth, J. A.; Htoon, H., ‘Giant’ CdSe/CdS Core/Shell Nanocrystal Quantum Dots As Efficient Electroluminescent Materials: Strong Influence of Shell Thickness on Light-Emitting Diode Performance. *Nano Lett.* **2012**, *12*, 331-336.
4. Meinardi, F.; Colombo, A.; Velizhanin, K. A.; Simonutti, R.; Lorenzon, M.; Beverina, L.; Viswanatha, R.; Klimov, V. I.; Brovelli, S., Large-Area Luminescent Solar Concentrators Based on ‘Stokes-Shift-Engineered’ Nanocrystals in a Mass-Polymerized PMMA Matrix. *Nat. Photonics* **2014**, *8*, 392-399.
5. Javaux, C.; Mahler, B.; Dubertret, B.; Shabaev, A.; Rodina, A. V.; EfrosAl, L.; Yakovlev, D. R.; Liu, F.; Bayer, M.; Camps, G.; Biadala, L.; Buil, S.; Quelin, X.; Hermier, J. P., Thermal Activation of Non-Radiative Auger Recombination in Charged Colloidal Nanocrystals. *Nat. Nanotechnol.* **2013**, *8*, 206-212.

6. Chen, Y.; Vela, J.; Htoon, H.; Casson, J. L.; Werder, D. J.; Bussian, D. A.; Klimov, V. I.; Hollingsworth, J. A., “Giant” Multishell CdSe Nanocrystal Quantum Dots with Suppressed Blinking. *J. Am. Chem. Soc.* **2008**, *130*, 5026-5027.
7. Bae, W. K.; Park, Y.-S.; Lim, J.; Lee, D.; Padilha, L. A.; McDaniel, H.; Robel, I.; Lee, C.; Pietryga, J. M.; Klimov, V. I., Controlling the Influence of Auger Recombination on the Performance of Quantum-Dot Light-Emitting Diodes. *Nat. Commun.* **2013**, *4*, 2661.
8. Park, Y.-S.; Bae, W. K.; Padilha, L. A.; Pietryga, J. M.; Klimov, V. I., Effect of the Core/Shell Interface on Auger Recombination Evaluated by Single-Quantum-Dot Spectroscopy. *Nano Lett.* **2014**, *14*, 396-402.
9. Kundu, J.; Ghosh, Y.; Dennis, A. M.; Htoon, H.; Hollingsworth, J. A., Giant Nanocrystal Quantum Dots: Stable Down-Conversion Phosphors that Exploit a Large Stokes Shift and Efficient Shell-to-Core Energy Relaxation. *Nano Lett.* **2012**, *12*, 3031-3037.
10. Bae, W. K.; Padilha, L. A.; Park, Y.-S.; McDaniel, H.; Robel, I.; Pietryga, J. M.; Klimov, V. I., Controlled Alloying of the Core–Shell Interface in CdSe/CdS Quantum Dots for Suppression of Auger Recombination. *ACS Nano* **2013**, *7*, 3411-3419.
11. García-Santamaría, F.; Chen, Y.; Vela, J.; Schaller, R. D.; Hollingsworth, J. A.; Klimov, V. I., Suppressed Auger Recombination in “Giant” Nanocrystals Boosts Optical Gain Performance. *Nano Lett.* **2009**, *9*, 3482-3488.
12. Park, Y. S.; Malko, A. V.; Vela, J.; Chen, Y.; Ghosh, Y.; García-Santamaría, F.; Hollingsworth, J. A.; Klimov, V. I.; Htoon, H., Near-Unity Quantum Yields of Biexciton

Emission from CdSe/CdS Nanocrystals Measured Using Single-Particle Spectroscopy. *Phys. Rev. Lett.* **2011**, *106*, 187401.

13. Mahler, B.; Spinicelli, P.; Buil, S.; Quelin, X.; Hermier, J.-P.; Dubertret, B., Towards Non-Blinking Colloidal Quantum Dots. *Nat. Mater.* **2008**, *7*, 659-664.

14. Zhao, J.; Chen, O.; Strasfeld, D. B.; Bawendi, M. G., Biexciton Quantum Yield Heterogeneities in Single CdSe (CdS) Core (Shell) Nanocrystals and Its Correlation to Exciton Blinking. *Nano Lett.* **2012**, *12*, 4477-4483.

15. Dai, X.; Zhang, Z.; Jin, Y.; Niu, Y.; Cao, H.; Liang, X.; Chen, L.; Wang, J.; Peng, X., Solution-Processed, High-Performance Light-Emitting Diodes Based on Quantum Dots. *Nature* **2014**, *515*, 96-99.

16. Lim, J.; Jeong, B. G.; Park, M.; Kim, J. K.; Pietryga, J. M.; Park, Y.-S.; Klimov, V. I.; Lee, C.; Lee, D. C.; Bae, W. K., Influence of Shell Thickness on the Performance of Light-Emitting Devices Based on CdSe/Zn_{1-x}Cd_xS Core/Shell Heterostructured Quantum Dots. *Adv. Mater.* **2014**, *26*, 8034-8040.

17. Matthews, J. W.; Blakeslee, A. E., Defects in Epitaxial Multilayers: I. Misfit Dislocations. *J. Cryst. Growth* **1974**, *27*, 118-125.

18. Adachi, S., *Handbook on Physical Properties of Semiconductors*. Kluwer Academic Publishers: Boston, **2004**; pp. 259.

19. Feng, S.; Wu, J.; Hu, P.; Chen, Y.; Ma, B.; Peng, J.; Yang, J.; Jiang, H., Epitaxial Growth of Successive CdSe Ultrathin Films and Quantum Dot Layers on TiO₂ Nanorod Arrays for Photo-Electrochemical Cells. *RSC Adv.* **2014**, *4*, 12154-12159.

20. Kane, E. O., Band Structure of Indium Antimonide. *J. Phys. Chem. Solids* **1957**, *1*, 249-261.
21. Cragg, G. E.; Efros, A. L., Suppression of Auger Processes in Confined Structures. *Nano Lett.* **2010**, *10*, 313-317.
22. Galeriu, C.; Lew Yan Voon, L. C.; Melnik, R.; Willatzen, M., Modeling a Nanowire Superlattice Using the Finite Difference Method in Cylindrical Polar Coordinates. *Comput. Phys. Commun.* **2004**, *157*, 147-159.